

Structure, dynamics, and rheology of colloid-polymer mixtures: From liquids to gels

M. Laurati,^{1,a)} G. Petekidis,² N. Koumakis,² F. Cardinaux,¹ A. B. Schofield,³ J. M. Brader,⁴ M. Fuchs,⁴ and S. U. Egelhaaf¹

¹*Condensed Matter Physics Laboratory, Heinrich-Heine University, Universitätsstr. 1, 40225 Düsseldorf, Germany*

²*IESL-FORTH and Department of Materials Science and Technology, University of Crete, 71110 Heraklion, Greece*

³*SUPA, School of Physics, The University of Edinburgh, Mayfield Road, Edinburgh EH9 3JZ, United Kingdom*

⁴*Soft Matter Theory Group, University Konstanz, 78457 Konstanz, Germany*

(Received 21 December 2008; accepted 2 March 2009; published online 3 April 2009)

We investigate the structural, dynamical, and viscoelastic properties of colloid-polymer mixtures at intermediate colloid volume fraction and varying polymer concentrations, thereby tuning the attractive interactions. Within the examined range of polymer concentrations, the samples varied from fluids to gels. In the liquid phase, an increasing correlation length of the density fluctuations when approaching the gelation boundary was observed by static light scattering and microscopy, indicating clustering and formation of space-spanning networks. Simultaneously, the correlation function determined by dynamic light scattering decays completely, indicating the absence of dynamical arrest. Clustering and formation of transient networks when approaching the gelation boundary is supported by significant changes in the viscoelastic properties of the samples. Upon increasing the polymer concentration beyond the gelation boundary, the rheological properties changed qualitatively again, now they are consistent with the formation of colloidal gels. Our experimental results, namely, the location of the gelation boundary as well as the elastic (storage) and viscous (loss) moduli, are compared to different theoretical models. These include consideration of the escape time as well as predictions for the viscoelastic moduli based on scaling relations and mode coupling theories. © 2009 American Institute of Physics. [DOI: 10.1063/1.3103889]

I. INTRODUCTION

The mechanical properties of solids and liquids are very different. A solid responds elastically to a small deformation, while a liquid flows. Complex fluids, such as colloidal suspensions, polymers, or surfactant solutions, have mechanical properties between those of elastic solids and viscous liquids, they are viscoelastic. Furthermore, they can be significantly perturbed by even modest mechanical forces. This causes a wealth of fascinating effects,¹ but is also a challenge to fundamental and applied research to understand their behavior under deformation and flow, i.e., their rheology. A detailed knowledge of their properties is crucial for many applications as complex fluids are extensively used in industrial products and processes.^{1,2}

Among complex fluids, colloidal suspensions are frequently used as models of atomic systems whose interparticle interactions can be tuned.^{3,4} These model systems allow the investigation of various fundamental phenomena, such as the equilibrium thermodynamics of gas, liquid, and crystal phases and also the nonequilibrium behavior of gels and glasses. The latter are disordered solids which are dynamically arrested and long-lived. Although they can be formed at any colloid volume fraction,^{5,6} most studies have focused on either very large or small volume fractions.

At low colloid volume fractions, the interparticle attraction induces the formation of clusters^{7–9} which may interconnect to create a space-spanning network.^{10–12} A connection between the gelation boundary and the spinodal line has been proposed^{13–18} with spinodal decomposition driving cluster formation and gelation.¹² The elasticity of gels is related to the connectivity of the network and the size of the clusters, i.e., to the heterogeneous structure of the network.^{10,19–21}

In contrast, at large volume fractions amorphous solids are already formed in the absence of attraction due to crowding and these are termed repulsive hard-sphere glasses.^{22,23} Increasing the attractive strength initially causes melting of the repulsive glass before, for even larger attractions, again an amorphous solid glass forms. However in this case it is the attractive bonding between the spheres which forms the glass and these are termed attractive glasses.^{24–26} Mode coupling theory (MCT) has shown that the formation of repulsive and attractive glasses is caused by dynamical arrest due to caging and bonding, respectively.^{24,26–29} These two arrest mechanisms seem to dominate also the mechanical response to deformations. The elastic properties are determined by the confinement of particles and can be rationalized in terms of the ratio between the energy and the volume characterizing the structural length of the system, which at high volume fractions coincides with the particle size.^{30,31} In addition, rheological and scattering experiments on repulsive^{32,33} and

^{a)}Electronic mail: marco.laurati@uni-duesseldorf.de.

attractive glasses^{34,35} indicated one (in the former) or two (in the latter) yielding steps related to cage and bond breaking.

In the region of intermediate colloid volume fraction the origin of the fluid-solid transition (even in the quiescent state) and the rheological properties of the amorphous solid are still under debate.^{36,37} By combining a macroscopic investigation of the phase diagram, rheology, and MCT calculations,^{31,38,39} the origin of the fluid-solid transition has been associated with dynamical arrest caused by bonding, in analogy with attractive glasses. This picture implies a sharp transition from nonbonded states (liquids) to bonded states (gels). However, the effect of bond lifetime on the transition has not yet been investigated. Recent simulations^{12,36} furthermore predict an important role of spinodal decomposition also at intermediate volume fractions.

The microstructure of liquids and gels at intermediate volume fractions has been characterized by scattering^{5,40,41} and confocal microscopy experiments.^{42–45} The microstructure of liquids can be well described, also in the presence of dispersed clusters, by an equilibrium theory based on the polymer reference interaction site model (PRISM).^{40,46} The structure of arrested gels is characterized by heterogeneities,^{42–45} whose characteristic size is maximum in the vicinity of the gelation boundary.^{43–45} Such structural heterogeneities coincide with dynamical heterogeneities^{43,45,47} and have significant effect on the rheological response of gels in the vicinity of the gelation boundary.³⁸ The gel elasticity therefore results from the combined effect of the interparticle bonds, as in attractive glasses, as well as the connectivity of the network, as in low volume fraction gels. The relative importance of these two effects at intermediate volume fractions and at semidilute polymer concentrations has not yet been clarified. It has been recently suggested that the micromechanical response of gels with different interparticle attractions is strongly correlated with the “clusterlike” or “stringlike” nature of the gel structure.⁴⁸

Here we are interested in this intriguing region of intermediate colloid volume fraction. In particular, we investigate the transition from liquidlike to solidlike behavior upon increasing interparticle attraction. We use a mixture of nearly hard-sphere colloidal particles with nonadsorbing linear polymer.^{5,14,49–51} The polymer induces a depletion attraction between the particles whose range and strength can be tuned by the polymer size and concentration, respectively. We investigate the static and dynamic properties of samples with an increasing polymer concentration, i.e., increasing strength of the attractive interaction. Upon increasing polymer concentration, the system evolves from an equilibrium liquid to a nonequilibrium, dynamically arrested gel.^{5,6,42,43,52,53} We use static and dynamic light scattering (DLS) and microscopy to investigate this liquid-solid transition and determine structural parameters, such as the characteristic correlation length of density fluctuations, and dynamic properties, such as the collective dynamics. The mechanical properties of the samples are probed through small amplitude oscillatory shear. This combination allows us to relate the static and dynamic properties in the quiescent samples to their linear viscoelastic response. We particularly focus on the following

TABLE I. List of samples. ϕ is the colloid volume fraction, c_p/c_p^* and c_p^{free}/c_p^* are the polymer concentrations in the total and free volume, respectively, in units of the overlap concentration, and ξ^* is the effective polymer-colloid size ratio.

c_p/c_p^* nominal	ϕ	c_p/c_p^*	c_p^{free}/c_p^*	ξ^*
0	0.40
0.1	0.40	0.10	0.21	0.079 ± 0.01
0.2	0.40	0.20	0.40	0.067 ± 0.009
0.25	0.40	0.25	0.49	0.063 ± 0.008
0.32	0.39	0.32	0.62	0.057 ± 0.007
0.4	0.40	0.40	0.76	0.052 ± 0.007
0.5	0.41	0.48	0.90	0.048 ± 0.006
0.7	0.40	0.70	1.28	0.040 ± 0.006
0.8	0.40	0.82	1.48	0.037 ± 0.005
1	0.40	0.99	1.78	0.033 ± 0.005
1.5	0.40	1.49	2.63	0.027 ± 0.004
2	0.40	1.99	3.48	0.023 ± 0.004

aspects of the fluid-solid transition and gel properties: First, in the linear viscoelastic regime we investigate the time (frequency) dependence of the shear moduli as a function of increasing attraction, i.e., on moving from liquidlike to solidlike samples and deeper into the gel. We compare macroscopic relaxation times, obtained from the linear viscoelastic spectra, to collective relaxation times determined by DLS and to bond lifetimes estimated on the basis of particle escape. Moreover, we compare the frequency dependence of the moduli in the liquid phase to MCT predictions. MCT has only recently been extended to describe dynamically arrested states under shear.^{54–62} Second, the evolution of the storage modulus as a function of increasing polymer concentration is determined. When going from the liquid into the gel region, we particularly investigate the behavior of samples close to the gelation boundary. Our results are compared to experimental data on a similar system³⁸ and MCT-PRISM predictions,³⁸ indicating qualitative and quantitative differences. Deep inside the gel region we relate the polymer concentration dependence of the storage modulus to that of the correlation length of density fluctuations, i.e., the degree of heterogeneity, using a model based on scaling arguments.

II. MATERIALS AND METHODS

A. Samples

We investigated mixtures of polymethylmethacrylate (PMMA) colloids and linear polystyrene (PS) (from Polymer Laboratories) dispersed *in cis*-decalin at a temperature $T = 23$ °C. The average hydrodynamic radius of the PMMA particles, $R = 137$ nm, was determined by DLS in the very dilute regime. The polydispersity of the colloids was not directly measured, but suppression of crystallization in quiescent and sheared colloidal dispersions indicates a polydispersity of about 12%. The radius of gyration of the PS (molecular weight $M_w = 132.9$ kg/mol) *in cis*-decalin, $r_g = 10.8$ nm, was estimated based on Ref. 63 and the polydispersity was cited as $M_w/M_n = 1.01$. In dilute solution, this implies a polymer-colloid size ratio $\xi = r_g/R = 0.079 \pm 0.013$. The effective polymer-colloid size ratio ξ^* (shown in Table I)

takes into account the concentration dependence of the polymer size and the mesh size in the semidilute regime. It has been calculated according to the generalized free volume theory (GFVT).^{64,65}

The colloid stock solution with volume fraction $\phi=0.6$ was prepared by redispersing spun-down sediments, whose volume fraction was estimated to be $\phi=0.67$ when taking polydispersity into account.⁶⁶ Polymer stock solutions were prepared by adding *cis*-decalin to dry polymer. Polymer concentrations c_p (mass/volume) were calculated from the weighed masses of the two components and their densities. Colloid-polymer mixtures were obtained by mixing appropriate amounts of colloid and polymer stock solutions. After mixing, samples were vigorously shaken using a vortex shaker, then homogenized over 3 days in a rotating wheel mixer. The compositions of the samples are summarized in Table I with the first column giving the nominal polymer concentration which is used to refer to samples in the following. The polymer overlap concentration c_p^* has been estimated by $c_p^*=3M_w/4\pi N_A r_g^3$. Values of ϕ and c_p refer to the total volume and c_p^{free} to the volume not occupied by colloids as estimated by GFVT.^{64,65,67} Samples were mixed and the light scattering or microscopy measurements performed within an hour to avoid effects due to aging (Sec. II D).

B. Light scattering

Due to the difference in refractive index n between PMMA and *cis*-decalin ($n_{\text{PMMA}}=1.49$, $n_{\text{dec}}=1.48$) the samples are turbid. Multiple scattering was suppressed and single scattered light recorded using a three-dimensional static and DLS instrument (LS Instruments).^{68,69} From the cross-correlation function we extracted the dynamic structure factor $f(Q, \tau)$ with the delay time τ , the modulus of the scattering vector $Q=(4n_{\text{dec}}\pi/\lambda)\sin(\theta/2)$, the scattering angle θ , and the laser wavelength $\lambda=633$ nm (22 mW HeNe laser from JDS Uniphase).

In static light scattering (SLS) experiments, the Q -dependence of the time-averaged intensity $\langle I(Q) \rangle$ was calculated from the time-averaged intensities recorded by the two detectors, $\langle I_a(Q) \rangle$ and $\langle I_b(Q) \rangle$, and the intercept β_{ab} of the cross-correlation function,

$$\langle I(Q) \rangle = \sqrt{\langle I_a^{(1)}(Q) \rangle \langle I_b^{(1)}(Q) \rangle} = \sqrt{\langle I_a(Q) \rangle \langle I_b(Q) \rangle} (\beta_{ab} / \beta_{ab}^{(1)}), \quad (1)$$

where the superscript “(1)” refers to quantities determined in the single-scattering regime. To achieve ensemble averaging, the sample was rotated continuously. Rotation does not affect β_{ab} , $\langle I_a(Q) \rangle$, or $\langle I_b(Q) \rangle$, but only the time dependence of $f(Q, \tau)$. Static structure factors $S(Q)$ were obtained from $\langle I(Q) \rangle$ taking into account the particle form factor (as determined in the dilute regime) and the transmission T of the sample,

$$S(Q) = \frac{\phi^{(d)} T^{(d)} I(Q)}{\phi T I^{(d)}(Q)}, \quad (2)$$

where the superscript (d) refers to quantities determined in the dilute regime. This assumes that all significant contributions to the scattering are due to the colloids, as shown in

Ref. 70 for similar colloid-polymer mixtures (see also Refs. 40 and 71).

C. Microscopy

Differential Interference Contrast (DIC) microscopy experiments were performed using a Nikon Eclipse 80i upright microscope with a Nikon 100 \times Plan Apo objective and a Canon EOS 30-D digital camera. Samples were loaded into a homebuilt cell: Two nr. 1 cover slips were glued onto a microscope slide, leaving a 3–4 mm wide channel between them. The channel was filled with the sample and a further nr. 1 cover slip used to cover the sample at the top and glue [UV-cure adhesive, Norland Optical Adhesive (NOA) 61] to seal the open ends of the channel.⁷²

D. Rheology

We used an ARES-HR rheometer with a force balance transducer 10FRTN1 and a cone-plate geometry (cone angle 0.044 rad, cone diameter 25 mm) which provides a constant strain throughout the sample. The geometry surfaces were mechanically roughened to avoid wall slip. To test reliability of the geometries with roughened surfaces, we compared results obtained with roughened and smooth surface geometries for samples where the presence of wall slip could be excluded. The agreement was found to be satisfactory. In dynamic measurements wall slip apparently has no effect in the linear viscoelastic regime, but dramatically affects measurements at large strain amplitudes in the nonlinear regime when the polymer concentration is comparable or larger than c^* . Here we only investigate the linear regime with strain amplitudes $0.001 \leq \gamma_0 \leq 0.02$, while the results in the nonlinear regime are discussed elsewhere.⁷³

In order to minimize solvent evaporation, a solvent saturation trap was used. The trap isolates the sample from the surrounding atmosphere by a fluid seal at the top and a permanent seal at the bottom. Solvent evaporation leads to a saturated atmosphere inside the enclosure.

In order to eliminate the effect of sample loading and aging, the following procedure was adopted: After loading, a dynamic strain sweep test was performed, i.e., the samples were subjected to oscillatory shear at a frequency of $\omega = 1$ rad/s and the strain amplitude γ_0 was increased until the sample showed a liquidlike response; $\gamma_0=8$ was sufficient at all c_p . Moreover, before each test, oscillatory shear with $\omega = 1$ rad/s and $\gamma_0=8$ was imposed on the samples until G' and G'' reached constant, steady-state values. Subsequently, samples were left at rest for a waiting time t_w before the test was started. We performed aging experiments: A series of dynamic time sweeps at $\omega=10$ rad/s and a total duration of 50 000 s without any rejuvenation in between. Samples below the macroscopic gelation boundary showed no aging effects over the whole time interval, while gels showed an initial increase of the elastic modulus within the first 200 s after loading, but then the moduli remained constant at least up to 3600 s. A detailed study of aging effects on the rheological properties of gels will be reported elsewhere.⁷⁴ Here we note that for $200 \text{ s} \leq t_w \leq 3600 \text{ s}$ the viscoelastic proper-

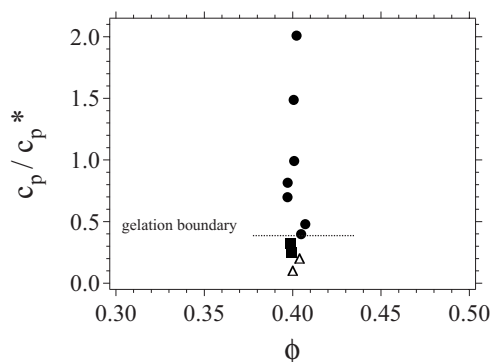


FIG. 1. Macroscopic behavior as investigated by tube inversion for different volume fractions ϕ and polymer concentrations c_p/c_p^* . (●) Gels (no flow), (■) highly viscous fluids, and (△) low viscosity fluids.

ties did not change and reproducible results were obtained in consecutive tests. We have chosen $t_w=300$ s.

III. RESULTS AND DISCUSSION

A. Quiescent samples

1. Macroscopic behavior

The macroscopic behavior of the samples was investigated by tube inversion as a function of colloid volume fraction ϕ and polymer concentration c_p/c_p^* (Fig. 1). Gel samples were identified by the absence of flow after tube inversion, which was found for $c_p/c_p^* \geq 0.4$. Samples with $0.2 < c_p/c_p^* < 0.4$ showed already a relatively high viscosity, but were still flowing.

2. Microscopic structure

Microscopic structural information were obtained by SLS and DIC microscopy. We determined the static structure factor $S(Q)$ at low scattering vectors $0.35 \leq QR \leq 2.6$ (Fig. 2) where length scales corresponding to large structures of the order of a few particle diameters are probed. Due to the limited Q -range we cannot observe the first peak of $S(Q)$ which for a pure colloidal dispersion with $\phi=0.4$ is expected, depending on polydispersity, in the range $3 < QR < 4$.^{40,75}

Below the macroscopic gelation boundary [$c_p/c_p^* < 0.4$, Fig. 2(a)], $S(QR < 1)$ monotonically increases with increasing c_p/c_p^* . For $c_p/c_p^* \leq 0.25$ a finite value of $S(Q \rightarrow 0)$ could be extrapolated which is consistent with the clustering of particles due to attractive depletion interactions, as has already been observed for silica-PS mixtures at the same colloid volume fraction.⁴⁰ These clusters are not necessarily equilibrium clusters.⁷⁻⁹ For larger polymer concentrations, $c_p/c_p^*=0.32$ and 0.4 , $S(QR < 1)$ increases steeply, which indicates an increasing amplitude of the concentration fluctuations, while crossing the gelation boundary ($c_p/c_p^* \approx 0.4$), $S(QR < 1)$ drops dramatically pointing at the suppression of large density fluctuations. Then $S(QR < 1)$ increases again inside the gel region, i.e., for $c_p/c_p^* > 0.4$ [Fig. 2(b)].

The c_p -dependence of $S(Q)$ at two distinct Q values ($QR=0.35$ and 0.7) is summarized in Fig. 3. The strong increase in $S(Q)$ upon approaching the gelation boundary, i.e., $c_p/c_p^* \leq 0.4$, can be described by a power-law dependence,

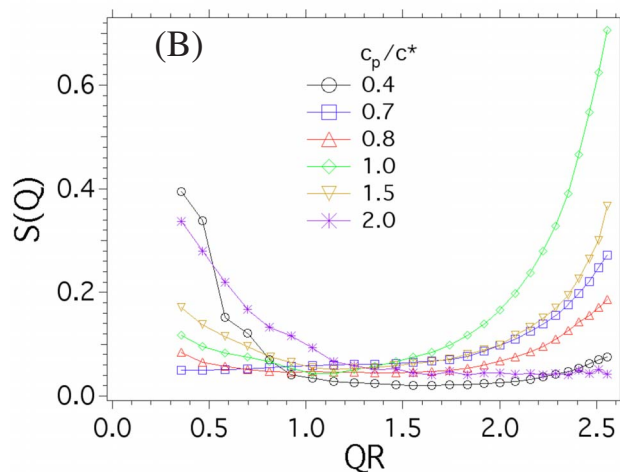
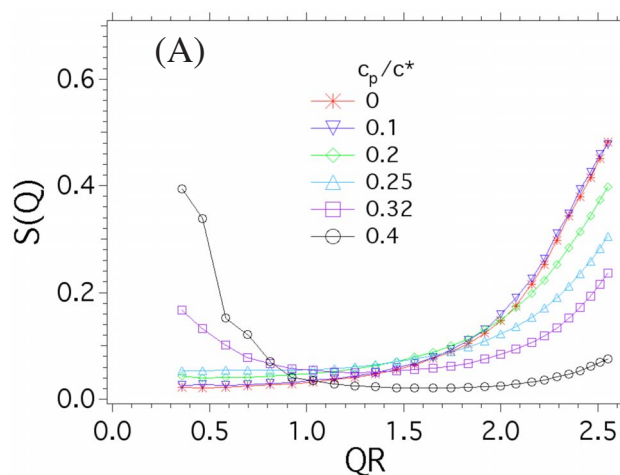


FIG. 2. (Color online) Static structure factor $S(Q)$ measured by SLS for different polymer concentrations c_p/c_p^* (as indicated in the legends) for samples below (a) and above (b) the macroscopic gelation boundary.

$S(Q) \sim (c_p/c_p^*)^\alpha$,⁴⁰ with an exponent $\alpha(QR=0.35)=4.6 \pm 0.3$ and $\alpha(QR=0.7)=2.6 \pm 0.1$. After the sharp drop at the gelation boundary, $S(Q)$ increases roughly linearly with increasing c_p/c_p^* inside the gel region.

A characteristic correlation length ζ can be extracted (Fig. 3, inset) by fitting an Ornstein–Zernike scaling, $S(Q) \sim 1/[Q^2 + (1/\zeta)^2]$ (Ref. 76) to those $S(QR < 1)$ which increase at low Q . We find that $\zeta/2R$ increases from approximately 1 to 6 upon increasing c_p/c_p^* from 0.32 to 0.4 and then, inside the gel region, drops again to approximately 1 with a slight increase with increasing c_p/c_p^* .

Due to the limited Q -range accessible in our light scattering experiments and, as a consequence, the large uncertainty in the value of ζ , we complemented our light scattering experiments by DIC microscopy (Fig. 3). At $c_p/c_p^*=0$ the sample appears homogeneous reflecting its fluid structure. Increasing c_p/c_p^* toward the gel boundary, some graininess due to large scale structures is visible with the length scale and amplitude increasing strongly at the gelation boundary ($c_p/c_p^*=0.4$). Within the gel phase ($c_p/c_p^* \geq 0.7$) the length scale and amplitude of the observed graininess decreases and subsequently saturates. DIC microscopy thus indicates that structural heterogeneities have a maximum around $c_p/c_p^* = 0.4$ and their length scale well before gelation and inside

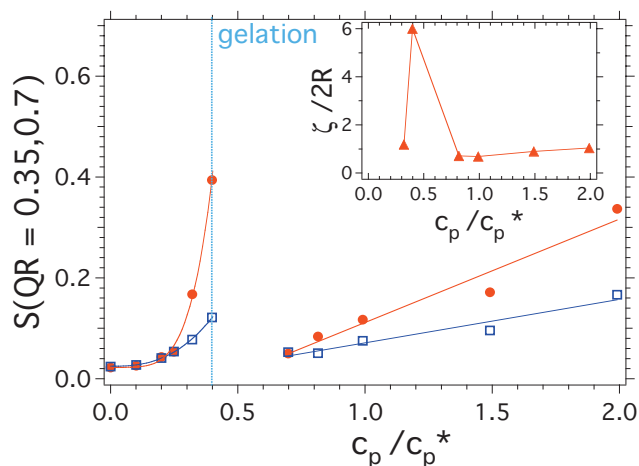


FIG. 3. (Color) Upper plot: static structure factor $S(Q)$ at $QR=0.35$ (red circles) and $QR=0.7$ (blue squares) as a function of polymer concentration c_p/c_p^* . Lines are fits by a power-law dependence for $c_p/c_p^* < 0.4$, and a linear dependence for $c_p/c_p^* > 0.4$. Inset: correlation length ζ obtained by fitting an Ornstein-Zernike scaling to the low Q part of $S(Q)$. Lower pictures: DIC microscopy images of samples with polymer concentrations $0 \leq c_p/c_p^* \leq 2$ as indicated.

the gel region appears to be comparable. This is consistent with our light scattering results. Note that for $c_p/c_p^*=0.7$ DIC microscopy allows us to observe large scale structures comparable in size to those observed for $c_p/c_p^*=0.4$. These large scale structures are not seen in SLS measurements due to the limited Q range accessible in experiments.

Large scale heterogeneous structures have been revealed by scattering experiments in silica-PS mixtures⁴⁰ and by confocal microscopy experiments for gels composed of polymer-grafted silica spheres⁴² as well as for dense PMMA-PS suspensions.^{43–45,77} While the degree of heterogeneity of the silica-PS mixture was found to remain approximately constant inside the gel phase,⁴⁰ confocal microscopy experiments on PMMA-PS suspensions^{43,45,77} present a trend of the degree of heterogeneity similar to the one observed here, with the maximum degree of heterogeneity ob-

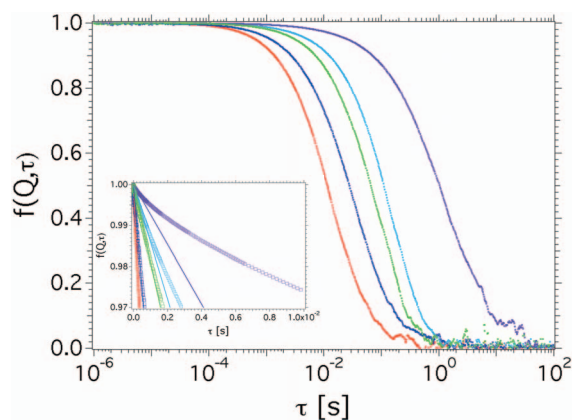


FIG. 4. (Color) Dynamic structure factor $f(Q, \tau)$ at $QR=0.7$ as a function of delay time τ for samples with polymer concentration $c_p/c_p^*=0$ (red), 0.1 (blue), 0.2 (green), 0.25 (turquoise), and 0.32 (violet; from left to right). Inset: initial decay of $f(Q, \tau)$. Lines are fits to the short-time expansion of $f(Q, \tau)$ derived from the Smoluchowski equation (Ref. 3).

served in the vicinity of the gelation boundary and a decreasing degree of heterogeneity inside the gel region. A relation between the presence of structural heterogeneities and the appearance of dynamical heterogeneities has been demonstrated in Refs. 43 and 45. The sharp maximum of the structural correlation length at the gelation boundary is expected for an arrested phase separation.³⁶ In this scenario, phase separation at the gelation boundary leads to a coarsening and cluster formation that is interrupted by dynamical arrest when the clusters permanently bond to form a gel. Due to our relatively large volume fraction, it is also conceivable that clusters connect to form a transient percolated network, which only arrests when the bond lifetime becomes large enough. To confirm that phase separation ultimately causes gelation is beyond the scope of this paper and requires a more detailed study, including an investigation of the time dependence of the low Q scattering after mixing.

3. Dynamics

DLS was performed with samples below the macroscopic gelation boundary ($c_p/c_p^* < 0.4$). Measurements were done at different scattering vectors Q , all of them below the first peak of the structure factor where the dynamic structure factor $f(Q, \tau)$ reflects collective dynamics. The data obtained at $QR=0.7$ are shown in Figs. 4 and 5. That $f(Q, \tau)$ completely decays indicates that the particle dynamics is ergodic, consistent with the macroscopic gelation boundary at $c_p/c_p^* > 0.32$. The decay of $f(Q, \tau)$ cannot be described by a single exponential: At short times it is exponential, while at long times it is stretched exponential. With increasing c_p particle dynamics slow down on both time scales (Fig. 4).

The initial fast decay of $f(Q, \tau)$ covers only about 3% of the total decay (Fig. 4, inset). At short times, individual particles diffuse freely as reflected in the linear time dependence. This linear dependence is described by the short-time limit expression derived from the Smoluchowski equation:³ $f(Q, \tau) = 1 - D_s(Q)Q^2\tau + O(\tau^2)$, where $D_s(Q)$ is the effective short-time diffusion coefficient. Departure from single relaxation related to short-time diffusion is observed at progressively shorter times for increasing c_p . This c_p -dependent de-

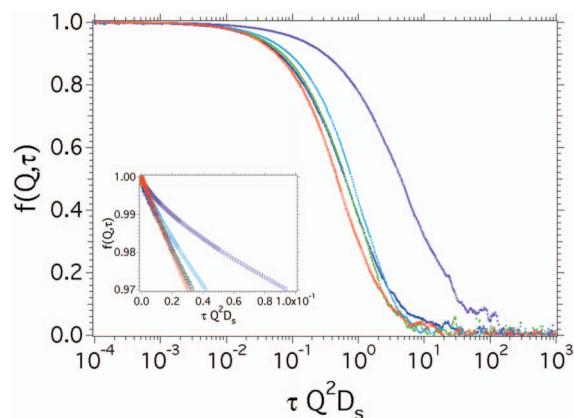


FIG. 5. (Color) Dynamic structure factor $f(Q, \tau)$ at $QR=0.7$ as a function of the rescaled delay time $\tau Q^2 D_s$ with the effective short-time diffusion coefficient D_s . Samples are as in Fig. 4. Inset: initial decay of $f(Q, \tau)$.

parture is clearly visible if $f(Q, \tau)$ is plotted as a function of the rescaled time $\tau Q^2 D_s$ (Fig. 5, inset). The rescaling with $D_s(c_p)$, whose Q -dependence is omitted here since Q is fixed, also accounts for the trivial dependence on the relative viscosity of the polymer solution $\eta_r = \eta(c_p)/\eta_s$ ($\eta(c_p)$ is the viscosity of the polymer solution, η_s is the solvent viscosity).

The long-time relaxation is also slowed down (Figs. 4 and 5). It corresponds to a collective, slow relaxation process related to the diffusion of particles whose movements are restricted by their mutual attraction. Its stretched form can be caused by size polydispersity, which leads to a spread in the long-time self-diffusion coefficients,³ and/or a distribution of particle diffusivities, caused by heterogeneities in the particle or cluster size distribution, in agreement with the SLS data (Fig. 3).

The short-time behavior for different Q is summarized in Fig. 6. Shown is the c_p -dependence of the normalized short-time diffusion coefficient $D_s(Q)\eta_r/D_0$ where $D_0 = k_B T / 6\pi\eta_{dec}R$ is the free diffusion coefficient and is also measured. It decreases with increasing Q and c_p , especially in the range $0 \leq c_p/c_p^* \leq 0.2$. These trends of $D_s(Q)\eta_r/D_0 = H(Q)/S(Q)$ result from a delicate balance between the structure factor $S(Q)$ and the hydrodynamic function $H(Q)$ [Figs. 6(b) and 6(c)]. $H(Q)$ quantifies the hydrodynamic resistance to motion: A small value of $H(Q)$ corresponds to large resistance and *vice versa*.³ $S(Q)$ has been determined by SLS (Fig. 2). It is almost constant for $c_p/c_p^* \leq 0.2$ and then decreases toward the gelation boundary, except for the smallest scattering vector, $QR=0.7$ [Fig. 6(b)]. Based on $D_s(Q)\eta_r/D_0$ and $S(Q)$, $H(Q)$ was calculated [Fig. 6(c)]. Except for the smallest Q , $QR=0.7$, $H(Q)$ decreases monotonically with increasing c_p , indicating that increasing attraction between particles induces higher hydrodynamic resistance to motion.

The values of $D_s(Q)\eta_r/D_0$ for small c_p/c_p^* , i.e., close to the pure hard-sphere case, are larger than 1 for all values of QR due to the dominant contribution of $H(Q)$ as compared to $S(Q)$, in agreement with previous data.³ This reflects the collective character of the dynamics that speed up compared to the dilute case due to increased osmotic compressibility of the concentrated suspension. Increasing attraction within

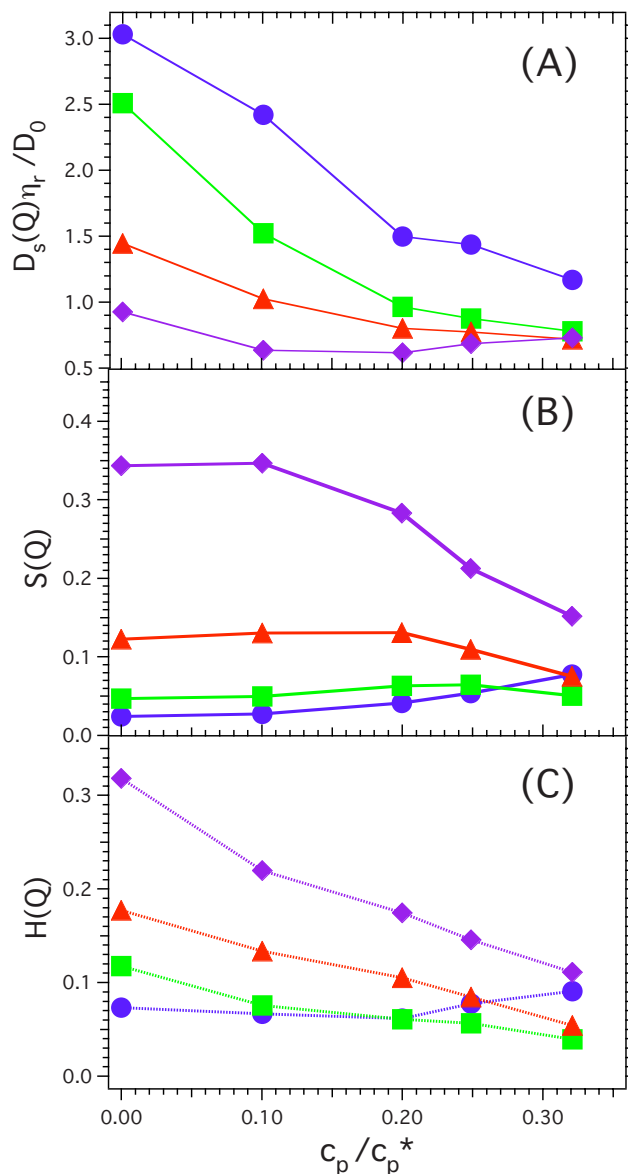


FIG. 6. (Color online) (a) Normalized short-time diffusion coefficient $D_s(Q)\eta_r/D_0$, (b) structure factor $S(Q)$, and (c) hydrodynamic function $H(Q)$ as a function of polymer concentration c_p/c_p^* for different scattering vectors $QR=0.7$ (●), 1.35 (■), 1.9 (▲), and 2.35 (◆).

$c_p/c_p^* \leq 0.2$ hardly affects the structure, hence $S(Q)$ is approximately constant, while it causes a decrease in $H(Q)$ which for $c_p/c_p^* \approx 0.2$ becomes smaller than $S(Q)$ resulting in a decrease in $D_s(Q)\eta_r/D_0$ to about 1. For larger polymer concentrations, $c_p/c_p^* \geq 0.2$, the particle attraction starts to affect the average structure with a reduction in $S(Q)$ near the peak (large QR) and an increase in $S(Q)$ at small QR due to aggregation [Fig. 2(a)]. Thus the trends of $H(Q)$ and $S(Q)$ become similar and $D_s(Q)\eta_r/D_0$ decreases toward a constant value. Only for the largest polymer concentration, the value of $D_s(Q)\eta_r/D_0$ remains approximately constant for $QR > 0.7$. Such a slowing down of the collective dynamics is a direct consequence of interparticle attractions. A similar trend has been observed in the liquid phase of a phase separating colloid-polymer mixture at comparable volume fractions in bulk and near a wall.⁷⁸

The normalized long-time diffusion coefficient

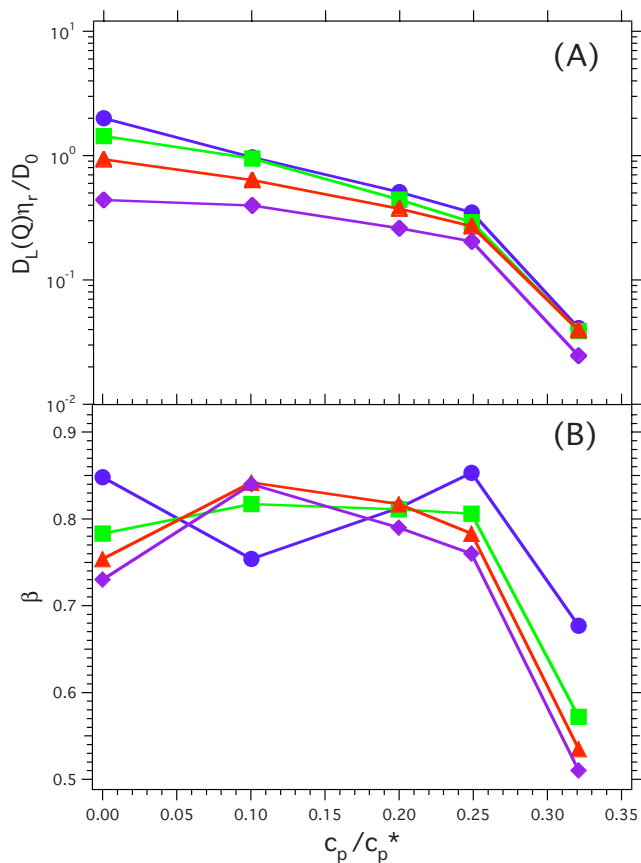


FIG. 7. (Color online) (a) Normalized long-time diffusion coefficient $D_L(Q)\eta_r/D_0$ and (b) stretching exponents β as a function of polymer concentration c_p/c_p^* for different scattering vectors $QR=0.7$ (●), 1.35 (■), 1.9 (▲), and 2.35 (◆).

$D_L(Q)\eta_r/D_0$ and stretching exponent β are obtained by fitting a stretched exponential to the long-time behavior of the dynamic structure factor (Fig. 7). $D_L(Q)\eta_r/D_0$ shows first a modest and then a sharp decrease with increasing c_p for all QR values. This indicates that particle attraction slows down particle motions and, in the vicinity of the gelation boundary ($c_p/c_p^* \lesssim 0.4$), the particles start to be localized, signaling the approach of dynamical arrest. The stretching exponent β is always below 1 with an approximately constant value of about 0.8 for $c_p/c_p^* < 0.25$ and a sharp decrease to about 0.5 at $c_p/c_p^* = 0.32$. This indicates that upon approaching the gelation boundary, density fluctuations increase, broadening the distribution of effective long-time collective diffusion coefficients, consistent with the increasing correlation length ζ of structural heterogeneities observed by SLS and microscopy (Fig. 3). The connection between structural and dynamical heterogeneities is supported by simulations⁴⁷ and confocal microscopy measurements on similar, less concentrated PMMA-PS mixtures.^{43,45}

B. Samples under shear

Dynamic frequency sweeps (DFSs) are reported in Fig. 8 for samples below (A) and above (B) the macroscopic gelation boundary, $c_p/c_p^* = 0.4$ (Fig. 1), with the frequency ω

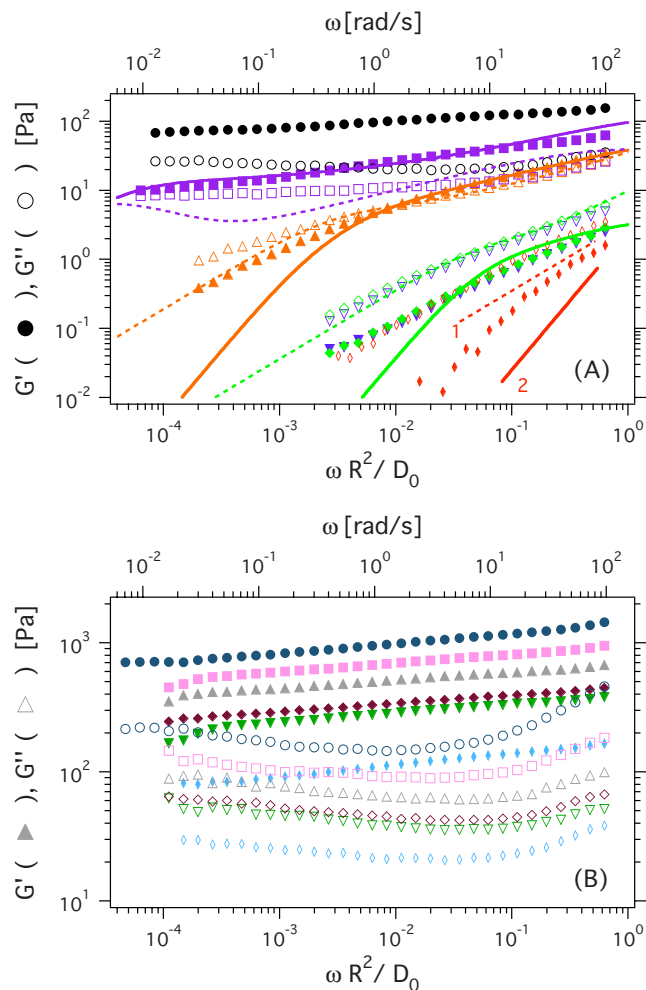


FIG. 8. (Color online) DFSs with elastic (storage) modulus G' (filled symbols) and viscous (loss) modulus G'' (open symbols) as a function of frequency ω in units of the instrument (top axis) and in units of the inverse diffusion time in the dilute limit $\tau_0 = R^2/D_0 \approx 4 \times 10^{-2}$ s (bottom scale). Samples below the macroscopic gelation boundary ($c_p/c_p^* \leq 0.4$) are shown in the upper, in the gel region ($c_p/c_p^* > 0.4$) in the lower plot with polymer concentrations $c_p/c_p^* = 0$ (◆), 0.1 (▼), 0.2 (◆), 0.25 (▲), 0.32 (■), 0.4 (●), 0.5 (◆), 0.7 (▼), 0.8 (◆), 1.0 (▲), 1.5 (■), and 2.0 (●). Lines are MCT predictions for G' (solid lines) and G'' (dashed lines) (Sec. IV B). The straight lines in (a) indicate the typical scaling in a Newtonian liquid, $G' \sim \omega^2$ and $G'' \sim \omega$.

given in rad/s (top axis) and in units of the Brownian diffusion time in the dilute limit $\tau_0 = R^2/D_0 \approx 4 \times 10^{-2}$ s (bottom axis).

Without polymer ($c_p/c_p^* = 0$), the response is characteristic for concentrated hard-sphere suspensions,⁷⁹ with viscous modulus G'' larger than the elastic one, G' , and a liquidlike frequency dependence. The elasticity is still finite though, i.e., $G' > 0$.

For $c_p/c_p^* = 0.1$ and 0.2, G'' still exceeds G' over the whole frequency range. However the mechanical moduli show the same frequency dependence, which can be described by a power law with an exponent of about 0.55. The larger G' compared to hard spheres arises from enthalpic contributions due to the interparticle attraction. The observed response shows interesting similarities to that measured in chemical and physical polymer gels, in particular, in partially cured or weakly cross-linked materials at the percolation

point.^{80–82} This suggests that already for $0.1 \leq c_p/c_p^* \leq 0.2$ a percolated network is formed. In contrast to chemical gels this network is transient since the lifetime of the physical bonds between colloids is finite with bonds dynamically forming and breaking. This dynamic, transient structure is consistent with an ergodic behavior indicated by the full relaxation of the dynamic structure factor $f(Q, \tau)$ (Fig. 4).

The first indication of a solidlike response is found at large frequencies for $c_p/c_p^*=0.25$, with the crossing point of G' and G'' at $\omega\tau_0=10^{-2}$. This corresponds to structural relaxation times in the experimental time window, in agreement with the fluidlike relaxation observed by DLS (Fig. 4). Due to the increasing strength of the attractions, the lifetime of the particle network becomes comparable to the examined time scale (or frequency) and is long enough to cause solidlike behavior at short times, corresponding to high frequencies.

For $c_p/c_p^*=0.32$ the frequency dependence of both, G' and G'' , becomes weaker and they cross close to the low frequency limit of the investigated frequencies. This solidlike response over almost all measured frequencies indicates, upon increasing c_p , an increase in the structural relaxation time with an increase in the lifetime of the network and the approach to dynamical arrest. This is consistent with the drop in the long-time diffusion coefficient (Fig. 7).

When the macroscopic gelation boundary ($c_p/c_p^*=0.4$) is crossed, the frequency dependence of G' and G'' is comparable at all c_p , which suggests a structural relaxation time consistently larger than the experimental observation time and particle dynamics which are arrested leading to nonergodic behavior. Thus, the percolated network lacks (measurable) structural relaxation and bonds between particles have very long lifetime. Increasing c_p further increases the elastic response as indicated by the increase in G' .

Within the gel region ($c_p/c_p^* \geq 0.4$), G'' presents a minimum at intermediate frequencies. This has already been observed for a large variety of so-called “soft glassy materials.”^{35,83–88} Such a minimum suggests long-time (low frequency) structural relaxation, α relaxation, inside the gel phase. Its frequency could be associated with a transition from β to α relaxation (both outside the experimental time window) and thus be related to the length scale over which particles diffuse before they reach the transient nonergodicity plateau between the two processes. Since the minimum stays at $\omega R^2/D_0 \approx 4 \times 10^{-2}$ up to $c_p/c_p^*=1$ and then shifts toward lower frequencies, this indicates a constant α relaxation time for gels up to $c_p/c_p^*=1$ and an increasing α relaxation time for $c_p/c_p^* > 1$.

The c_p -dependence of the elastic modulus G' is shown in Fig. 9. Three different regimes can be distinguished. For $c_p/c_p^* < 0.25$ (region I in the figure), G' is very small and modestly increases with increasing c_p . (At the lowest frequency $\omega=0.1$ rad/s, G' could not be detected for $c_p/c_p^* < 0.25$.) For a fixed ω and increasing c_p , G' increases as a result of the increasing bond energy and the increasing contribution from slow density fluctuations. The density fluctuations will be averaged out at long times and will thus not contribute at low frequencies. Moreover, due to the low c_p the bond lifetime is short and there will be also no bond

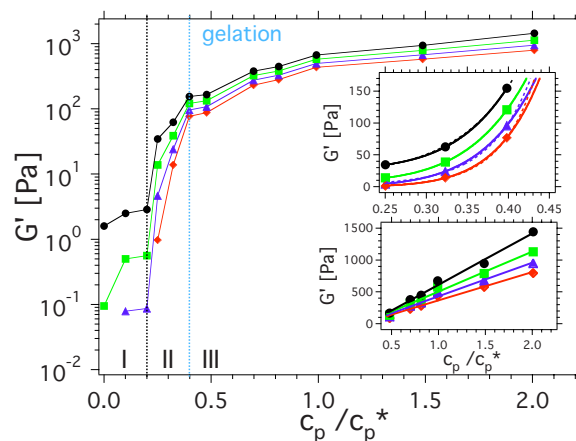


FIG. 9. (Color online) Elastic (storage) modulus G' extracted from DFSs as a function of polymer concentration c_p/c_p^* at different frequencies $\omega = 0.1$ rad/s (\blacklozenge), 1 rad/s (\blacktriangle), 10 rad/s (\blacksquare), and 100 rad/s (\bullet). Upper inset: G' as a function of c_p/c_p^* approaching gelation ($0.25 \leq c_p/c_p^* \leq 0.4$). Solid lines represent power-law fits with exponents from about 6.2 (red) to about 8.3 (black). Dashed lines represent exponential fits. Lower inset: G' as a function of c_p/c_p^* inside the gel phase ($c_p/c_p^* \geq 0.5$). Lines represent linear fits.

contribution to G' at long times (low frequencies). In contrast, at higher frequencies both contributions are present and G' thus increases with frequency.

Approaching the gelation boundary, $0.25 \leq c_p/c_p^* \leq 0.4$ (region II in the figure), G' shows a steep increase with increasing c_p (Fig. 9, upper inset), which reflects the strongly increasing number of permanent bonds and their increased strength which leads to a permanent, stress bearing network. The increase in G' can be described by a power law or exponential dependence. The exponent of the power-law dependence increases from about 6.2 to about 8.3 with decreasing frequency. Thus, the power-law dependence tends to the exponential dependence and hence the quality of the exponential fit improves with decreasing frequency. A more pronounced increase of G' with decreasing frequency is reminiscent of the discontinuous jump from zero to a finite shear modulus when crossing the gelation boundary as predicted by MCT.²⁶ In Sec. IV B we compare these data to MCT predictions, which take the bond energy into account, but neglect effects of heterogeneous structure and percolation.

Within the gel region, $c_p/c_p^* \geq 0.5$ (region III in the figure), G' increases linearly (Fig. 9, lower inset). In the gel the network is persistent and saturation of permanent bonds is reached, therefore the elasticity of the gel depends on the structure of the network (open or compact clusters) and the bond energy. A simple model which accounts for both contributions is proposed below (Sec. IV D).

The DFSs and the dependence of the elastic modulus G' on polymer concentration c_p together with the DLS results and macroscopic observations indicate the existence of two transitions: First, at $c_p/c_p^*=0.25$ network formation and the first solidlike response with a relaxation time within the experimental time window is observed. Second, at $c_p/c_p^*=0.4$ gel formation and a solidlike response with a structural relaxation time outside the experimental time window was found. While both processes imply a network structure, the

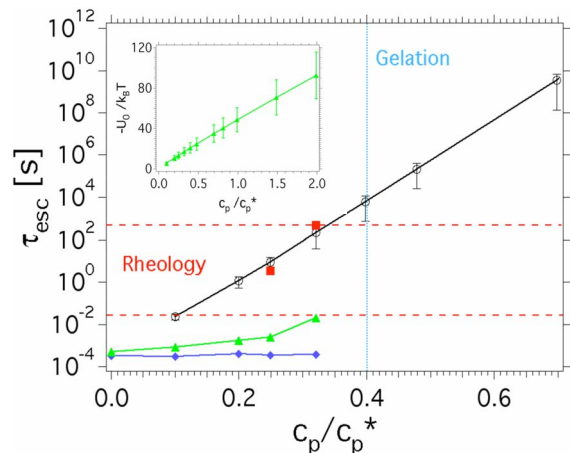


FIG. 10. (Color online) Escape time τ_{esc} for a particle confined to a linear ramp potential $U(r)$ as a function of polymer concentration c_p/c_p^* . τ_{esc} was calculated according to Eq. (4) (○) and compared to the time at which, according to rheology experiments, G' and G'' cross (■), and to the short (◆) and long (▲) relaxation times obtained from light scattering at $QR = 0.7$. Dashed red lines indicate the time window accessible by rheology. Inset: dependence of U_0 on c_p/c_p^* . Line is a fit to the power-law dependence $U_0 \sim (c_p/c_p^*)^{0.9}$.

dynamics of the networks, in particular, the lifetime of particle bonds and hence of the whole networks, are different.

IV. THEORETICAL MODELING

A. Bond lifetime

Our results suggest that a crucial parameter is the time particles remain within the range of their mutual attraction, i.e., the “bond” lifetime. This determines whether, on a given time scale, the network is transient or permanent. We estimate the bond lifetime as a function of polymer concentration c_p with a simple model based on Kramers approach⁸⁹ to describe the escape of particles from a potential well. The first passage time of a Brownian particle within a depletion potential (Asakura–Oosawa potential) can be calculated numerically.⁹⁰ In order to obtain an analytical expression, we approximate the depletion potential by a ramp potential $U(r)$ with the same depth U_0 ($U_0 < 0$) and width $\delta^* = 2\xi^*R$,

$$U(r) = \begin{cases} \infty, & r \leq 2R \\ U_0 \left(1 - \frac{r-2R}{2\xi^*R} \right), & 2R < r \leq 2(\xi^* + 1)R \\ 0, & r > 2(\xi^* + 1)R. \end{cases} \quad (3)$$

Based on the depletion potential we estimate $U_0 = -\Pi_p V_o(2R)$, where Π_p is the osmotic pressure and $V_o(r)$ the overlap volume of the depletion regions of two particles at distance r . We calculated V_o according to the GFVT,^{64,65,67} which accounts for the c_p -dependence of the polymer size and osmotic pressure (Sec. II A). The dependence of U_0 on c_p/c_p^* is shown in Fig. 10 (inset). The error bars reflect the uncertainty in the size ratio ξ^* , which results from the uncertainty in the colloid and polymer radii. This uncertainty propagates to an uncertainty in the escape time. The escape time τ_{esc} from a ramp potential is^{44,90}

$$\begin{aligned} \tau_{\text{esc}} &= \frac{1}{D_S^{(s)}} \int_0^{\delta^*} dx' e^{\beta U(x')} \int_{-\infty}^{x'} dx e^{-\beta U(x)} \\ &= \frac{\delta^{*2}}{D_S^{(s)}} \frac{e^{-\beta U_0} - (1 - \beta U_0)}{(\beta U_0)^2}, \end{aligned} \quad (4)$$

where $D_S^{(s)}$ is the short-time self-diffusion coefficient of a particle within the potential $U(r)$. It is estimated based on the short-time self-diffusion coefficient of a hard-sphere colloidal dispersion at $\phi = 0.4$; $D_S^{(s)} \approx 0.3D_0$.³ Since the ramp potential overestimates the particle attraction in a depletion potential, τ_{esc} is expected to overestimate the escape time for a depletion potential.

The escape time τ_{esc} increases rapidly with increasing c_p (Fig. 10). At $c_p/c_p^* \approx 0.4$ it reaches laboratory time scales (hours) and thus indicates permanent bonding and dynamical arrest and gel formation, in agreement with the macroscopic gelation boundary (Fig. 1). For $0.1 \leq c_p/c_p^* \leq 0.32$, τ_{esc} is within the experimental time window of the rheological measurements. In the rheology experiments we observe, within the accessible time window, a transition to solidlike behavior for $c_p/c_p^* = 0.25$ and 0.32 (Fig. 8). The frequency of the crossing point of G' and G'' (Fig. 10, filled squares) has the same order of magnitude as the calculated τ_{esc}^{-1} . This indicates that upon approaching gelation particles form a network whose relaxation time, given by the lifetime of the particle bonds, determines the structural relaxation of the system. For larger c_p , τ_{esc} and the crossing point of G' and G'' is beyond the time window accessible by rheology. For smaller polymer concentrations, $0 \leq c_p/c_p^* \leq 0.2$, no crossing point was observed, although the calculated τ_{esc} lies within the time window accessible by rheology. This suggests that in these samples the structural relaxation probed by rheology is not related to the breaking of particle bonds and the samples are rather fluids of individual particles or clusters of particles than transient network structures.

Based on the light scattering results, namely the short and long-time collective diffusion coefficients [Figs. 6(a) and 7(a)], we estimate the characteristic relaxation times on a length scale corresponding to the range of the potential, δ^* , $\tau_S = \delta^{*2}/D_S^{(s)}(Q)$ and $\tau_L = \delta^{*2}/D_L^{(s)}(Q)$ and compare them to τ_{esc} . The ratio between the short-time self-diffusion coefficient, $D_S^{(s)}$ and the collective diffusion coefficient for hard spheres with $\phi = 0.4$ as determined by DLS is $D_S^{(s)}/D_S \approx 0.2$.³ Since attraction mainly affects the long-time decay, we use this ratio as an estimate for all c_p (Fig. 10, filled diamonds). Its slight increase, almost invisible on the large vertical scale of the plot, is related to the c_p -dependence of the potential range δ^* . However, this τ_S is much smaller than the calculated τ_{esc} . For the long-time diffusion coefficient, $D_L^{(s)}/D_L \approx 0.1$ for hard spheres.³ In this case, this relation is only valid at small c_p , since large c_p , i.e., strong attraction, slows down the long-time self-diffusion due to bonding (in analogy to repulsive and attractive glasses^{24,70}). This is consistent with the agreement observed at $c_p/c_p^* = 0$, but τ_L increasingly underestimates the time needed to diffuse a distance δ^* , possibly being responsible for the increasingly large discrepancy between τ_L and τ_{esc} when approaching the gelation boundary (Fig. 10, filled triangles). Moreover, we found that for

$c_p/c_p^*=0.1$ and 0.2 the rheological relaxation time is faster than the shortest time accessible in the experiments and might thus be closer to τ_S than τ_{esc} . We attribute this to the fact that particles or particle clusters diffuse within a shorter time than the lifetime of particle bonds. This supports the above finding that samples with $c_p/c_p^* \leq 0.2$ are fluids of individual particles or particle clusters rather than transient or permanent networks, which start to form for $c_p/c_p^* \geq 0.25$.

Finally, long-time structural relaxation in samples inside the gel region is suggested by the minimum observed in G'' . In the gel region the bonds are so strong that they can be considered as essentially permanent (corresponding to huge τ_{esc} at $c_p/c_p^* > 0.4$, Fig. 10). The long-time relaxation can thus not be related to bond breaking, but might be associated with particles of different mobilities, as suggested by studies on dynamical heterogeneities,^{43,47} or with different restructuring processes, such as rotation of particle groups, which then lead to the observed stress relaxation and aging.

B. Frequency dependence of the moduli by mode coupling theory

MCT allows the shear modulus $G(t)$ to be calculated for dense colloidal suspensions and predicts the existence of a glass transition.^{55,91} Within this approach, the modulus is approximated by calculating the overlaps of stress fluctuations with density fluctuations in order to capture the slow structural relaxation which occurs close to the glass transition. The slow relaxation of the system is thus described by the transient density correlator. While the full mode coupling equations possess a wavevector dependence it has been shown for the quiescent case^{55,91} that a simplified, schematic version of the theory in which the Q -dependence is neglected can effectively capture the essential physics. Recent developments generalizing the theory to the case of steady-shear have shown that a similar schematic model can be used to represent the full mode coupling equations under shear, the so-called $F_{12}^{(\dot{\gamma})}$ model.⁵⁴⁻⁵⁶ Within this schematic model the transient density correlator $\phi(t)$ obeys the equation of motion

$$\partial_t \phi(t) + \Gamma \left(\phi(t) + \int_0^t dt' m(t-t') (\partial_{t'} \phi(t') + \delta \phi(t')) \right) = 0, \quad (5)$$

where $m(t)$ is the memory function, Γ is the initial decay rate and $\phi(0)=1$. Introduction of the parameter δ provides an additional decay mechanism leading to long-time relaxation of glassy states.⁹¹ The theory assumes that $m(t)$ and the shear modulus $G(t)$ relax on the same time scale as the correlator $\phi(t)$, therefore a self-consistent approximation closing the equations of motion can be made. In the $F_{12}^{(\dot{\gamma})}$ model the memory function $m(t)$ is given by

$$m(t) = \frac{1}{1 + (\dot{\gamma}t)^2} (v_1 \phi(t) + v_2 \phi^2(t)), \quad (6)$$

where v_1 and v_2 are coupling vertices chosen so as to reproduce the generic behavior of the full, Q -dependent theory at the glass transition and are thus not independent, but connected by a simple algebraic relation.⁵⁴⁻⁵⁶ Typically the pa-

rameters are chosen as $v_2=2$ and $v_1=v_2(\sqrt{4/v_2}-1) + \epsilon/(\sqrt{v_2}-1)$. In this way, both v_1 and v_2 are determined by the separation parameter ϵ . The value $\epsilon=0$ corresponds to the glass transition point and positive (negative) values of ϵ correspond to state points in the glass (fluid). Therefore ϵ and consequently v_1 and v_2 can be adjusted in relation to reproduce the dynamics as a function of the distance from the experimental gelation boundary. We note that for small amplitude oscillatory shear the $\dot{\gamma}$ dependence in $m(t)$ may be neglected. The modulus $G(t)$ is given in the $F_{12}^{(\dot{\gamma})}$ model by

$$G(t) = v_\sigma (\phi^2(t) + \tilde{x} \delta), \quad (7)$$

where the modulus amplitude v_σ provides an additional fit parameter used to reproduce the magnitude of the experimental elastic modulus. The elastic (storage) modulus G' and viscous (loss) modulus G'' are obtained by Fourier transformation

$$G'(\omega) + iG''(\omega) = i\omega \int_0^\infty dt e^{-i\omega t} G(t)_{\dot{\gamma}=0}. \quad (8)$$

In order to model the data, there are four free parameters: $\epsilon, \tilde{x}, v_\sigma$ and Γ . On a double logarithmic plot the shape of $G'(\omega)$ and $G''(\omega)$ depends only on the distance from the glass transition, parametrized by ϵ , and on the parameter \tilde{x} . The initial decay rate Γ and amplitude v_σ allow for horizontal and vertical translations, respectively. The additional decay parameter δ may then be used to fine tune $G''(\omega)$ at low frequencies.

The fundamental assumption of MCT is the description of dynamical arrest in terms of glassy dynamics, i.e., the slowing down of particle dynamics is caused by increasing caging of particles when approaching the glass transition. This limits the range of c_p , i.e., the strength of attraction, to which the model can be applied, namely, the region approaching the gel transition. For low polymer concentrations, $c_p/c_p^* < 0.2$, the dynamics are not adequately described in terms of caging. For large c_p/c_p^* , i.e., inside the gel region, the model cannot reproduce the frequency dependence of G' and G'' due to the different nature of the dynamics assumed in the model (glassy) and present in the samples.

Predictions based on the $F_{12}^{(\dot{\gamma})}$ model for the region where it is assumed to be valid, namely approaching the gel transition ($c_p/c_p^*=0.2, 0.25$ and 0.32), are shown in Fig. 8 (lines). Theory correctly estimates the relative magnitude of G' and G'' in the high frequency limit, in particular, for $c_p/c_p^*=0.25$, while an increasingly larger discrepancy evolves at lower frequencies. MCT associates a Newtonian fluid response to the system after structural relaxation, i.e., at frequencies below the crossing of G' and G'' , while the experimental response shows a less pronounced frequency dependence for both moduli. This could be caused by polydispersity and/or dynamical heterogeneities, which MCT does not consider but are indicated by the stretched exponential decay observed in DLS (Sec. III A 3). For $c_p/c_p^*=0.32$, G' agrees well with experiments, while the predicted G'' shows a consistently different frequency dependence. The predicted minimum appears only as a shoulder (at higher frequencies than the predicted minimum) in the experimental

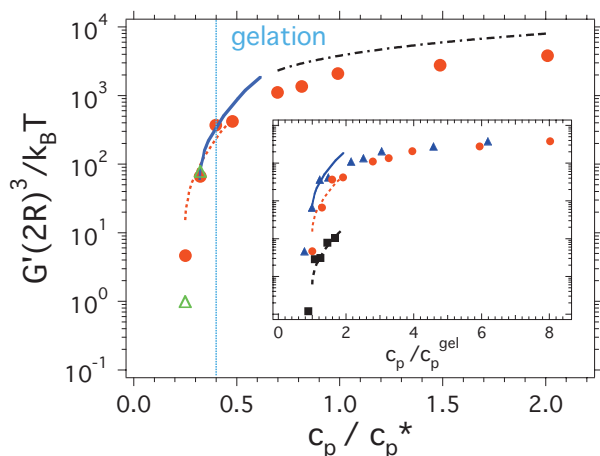


FIG. 11. (Color) Elastic modulus G' as a function of polymer concentration c_p/c_p^* . G' has been normalized by the particle volume $(2R)^3$ and the thermal energy $k_B T$. The experimentally determined G' has been extracted from DFSs at the lowest measured frequency, $\omega=0.1$ rad/s, (●) and is compared to $F_{12}^{(\gamma)}$ (△) and MCT-PRISM predictions for $G'(\omega \rightarrow 0)$. The red dotted line is the MCT-PRISM prediction obtained for $c_p^{\text{gel}}=0.25c_p^*$ and a scaling factor about 1/4. The solid line is the MCT-PRISM prediction obtained for $c_p^{\text{gel}}=0.32c_p^*$ and no scaling factor. The black dashed-dotted line indicates the slope $G' \sim (c_p/c_p^*)^{0.9}$. Inset: G' as a function of c_p/c_p^{gel} , for $c_p^{\text{gel}}=0.25c_p^*$ (●) and $c_p^{\text{gel}}=0.32c_p^*$ (▲). Red dotted and blue solid lines are the corresponding MCT-PRISM predictions. Measurements obtained for silica-PS mixtures with $\xi=0.09$ (■) from Ref. 38 are shown for comparison, with the corresponding (rescaled) MCT-PRISM predictions (black dashed line). Y-axes are identical in the main figure and inset.

data. This minimum reflects the presence of an α relaxation in the theoretical dynamics, which is in qualitative agreement with the rheological response (Fig. 8). We attribute the quantitative discrepancy of the relaxation times and of the detailed frequency dependence to the above mentioned differences between the dynamics of the experimental system and the glassy dynamics implicit in the theoretical model.

C. Polymer concentration dependence of the elastic modulus by mode coupling theory

In addition to the full frequency dependence discussed above, we now consider the c_p -dependence of the elastic modulus G' at a fixed (low) frequency ω . We compare our experimental data obtained for $\omega=0.1$ rad/s (Fig. 11, filled circles) to MCT predictions based on the $F_{12}^{(\gamma)}$ model as above (open triangles), and MCT-PRISM predictions.^{38,46} MCT-PRISM was recently applied to silica spheres-PS mixtures at volume fraction $\phi \approx 0.4$ and shown to correctly reproduce the c_p -dependence of the measured $G'(\omega=1$ Hz) over a range of c_p .³⁸ In this study, a gel was experimentally defined on the basis of rheological measurements as a sample for which $G'(\omega=1$ Hz) $> G''$ and $G' > 10$ Pa. Applied to our measurements this definition implies a gelation boundary at $c_p/c_p^*=0.25$. [In contrast, according to our criterion for a gel, the sample with $c_p/c_p^*=0.25$ is not considered a gel because it still shows structural relaxation (Fig. 4) and thus a fluidlike response.] The range of polymer concentrations investigated in Ref. 38 should thus be compared to $0.25 \leq c_p/c_p^* \leq 0.5$ in our measurements, i.e., in the vicinity of “our” gelation boundary.

MCT-PRISM predictions for G' (Fig. 11, blue solid line in the inset) are considerably larger than our experimental data. In order to compare the functional dependence we rescaled the theoretical predictions. The best match with the experimentally observed trend was obtained for a scaling factor of about 1/4 (dotted red line). This results in fair agreement; the increase in the experimentally observed G' is slightly more pronounced than predicted. A scaling factor was already proposed earlier³⁸ to account for the difference in the structure assumed in MCT-PRISM, a homogeneous fluid, and the silica-PS gels, which show structural heterogeneities in small-angle x-ray scattering experiments.⁴⁰ Structural heterogeneities are also present in our samples with $c_p/c_p^* > 0.25$ according to our SLS and DIC microscopy experiments (Figs. 2 and 3). The scaling factor giving quantitative agreement between experimental data and MCT-PRISM predictions was calculated from the ratio between the particle density and the density of particle clusters (with a size corresponding to the characteristic length of structural heterogeneities).³⁸ The characteristic length of structural heterogeneities, derived from scattering experiments,⁴⁰ remained constant with increasing c_p for silica-PS gels. In our case one has to assume a particle cluster size of about 1.6 particle diameters to obtain the ratio 1/4 between the particle density and the cluster density. Such particle cluster size lies between the characteristic correlation length ζ obtained for $c_p/c_p^*=0.32$ and $c_p/c_p^*=0.4$ from scattering experiments (Fig. 3), where ζ shows a strong c_p -dependence within the range of interest $0.25 \leq c_p/c_p^* \leq 0.5$. Nevertheless, rescaling the MCT-PRISM predictions by our $\zeta(c_p)$ makes the agreement between MCT-PRISM predictions and our experimental data worse (not reported here). The connection between the scaling factor (here 1/4) and the characteristic cluster size is therefore less clear in our system than in silica-PS gels.

There is some ambiguity in the determination of the gelation boundary. If we choose $c_p/c_p^*=0.32$ instead of 0.25, this would possibly agree better with the definition of the gelation boundary by the theory, namely, the transition from zero to a finite value of G' . Moreover, this shift might be justified by differences in the structure factor between the silica-PS mixtures and our samples. With a gelation boundary at $c_p/c_p^*=0.32$, no scaling factor is needed (Fig. 11, blue solid line). For $0.32 < c_p/c_p^* < 0.5$ the MCT-PRISM predictions describe the data well, while there are considerable discrepancies for $c_p/c_p^* > 0.5$ and no data for larger c_p/c_p^* are available for comparison.³⁸ They might be due to the difficulty to treat nonequilibrium states well inside the gel region or to account for the changes in attraction range and strength beyond the overlap concentration c_p^* . In order to evidence the sensitivity of the comparison between experimental data and MCT-PRISM predictions to the definition of the gelation boundary, the elastic modulus and theory predictions are plotted as a function of c_p/c_p^{gel} in the inset of Fig. 11. Two different values of c_p^{gel} , $0.25c_p^*$ (●) and $0.32c_p^*$ (▲) are used. Experimental data obtained for silica-PS mixture and rescaled MCT-PRISM predictions ($\xi=0.09$, ■ and black dashed line) are reported for comparison.³⁸ While agreement in the functional dependence between experiments and theory is obtained for both

systems within a comparable range of polymer concentrations, the agreement in the magnitude is strongly influenced by the choice of the gelation boundary.

These comparisons indicate that MCT and MCT-PRISM do not entirely capture the mechanisms responsible for the evolution of the shear moduli approaching and entering the gel region. Structural heterogeneities contribute to the observed discrepancies in both cases: First, structural heterogeneities might induce dynamical heterogeneities, which are not included in the glassy dynamics of the $F_{12}^{(j)}$ model. Second, the MCT-PRISM model is based on structure factors of fluidlike equilibrium structures, not heterogeneous nonequilibrium structures. However, the effect of structural heterogeneities seems not limited to a rescaling of the unit of stress transmission (a cluster instead of a single particle), in contrast to what is observed for silica-PS mixtures. Taking into account the polymer concentration dependence of the size of heterogeneities reduces the agreement. At the same time, shifting the gelation boundary according to our different definitions of c_p^{gel} , no rescaling of the moduli is needed (Fig. 11, inset). These two observations suggest differences in the routes leading to gelation between our system and silica-PS mixtures. The origin of these differences is so far unknown. However, they might result from a number of small differences such as different interactions between polymers and particles due to dissimilar chemical properties of the particle surface, or contrasting degrees of “softness,” which might become important for small particle separations, or an uneven influence of gravity due to a variation in the degree of density mismatch and size. The intrinsic distinction between the two systems is also evidenced by the unequal magnitude of the elastic moduli after rescaling by the particle volume (Fig. 11, inset).

D. Polymer concentration dependence of the elastic modulus inside the gel region

The structure of a gel can be considered as closely packed fractal clusters.^{10,92} We estimate the effect of changes in this microscopic structure on the c_p -dependence of the elastic properties. For large clusters, the elastic behavior of the gel will be dominated by the deformation of clusters (strong-link regime) and the elastic constant of a cluster, K_ζ , is expected to depend on the size of its backbone, i.e., decreases with increasing cluster size. For small clusters, intercluster links will deform before clusters deform (weak-link regime). The number of particle-particle links between clusters is smaller than the average number of particle bonds inside a cluster, as evidenced by confocal microscopy measurements of similar colloidal gels.^{44,77} Hence the elastic constant of the system will be dominated by the elastic constant of intercluster links, K_l . In both cases, the total elastic constant scales as $G \sim K/\zeta$.^{92–94}

Due to the large colloid volume fraction $\phi \approx 0.4$, our gels consist of small clusters (Fig. 3) and hence are expected to be in the weak-link regime. To obtain a scaling relation between G' and c_p , we have to determine the c_p -dependence of K_l and ζ . The correlation length ζ sharply decreases just above the gelation boundary but then remains approximately

constant well inside the gel region (Fig. 3). In a minimal model, the elastic constant of intercluster links, K_l , is expected to depend on the number m of particle-particle contacts between clusters and the interaction between two particles at contact, U_0 , i.e., $K_l \sim mU_0$. We assume that m does not depend on c_p . The c_p -dependence of U_0 (Fig. 10, inset) can be fitted by a power-law dependence, $U_0 \sim (c_p/c_p^*)^{0.9}$, inside the gel region. This results in $G' \sim K_l/\zeta \sim mU_0/\zeta \sim U_0 \sim (c_p/c_p^*)^{0.9}$. This scaling is in agreement with $G'(c_p)$ observed in experiments (Fig. 11, straight solid line). Therefore, this simple model seems to capture the essential mechanism leading to the elasticity of the gels, namely, the intercluster links.

V. CONCLUSIONS

We investigated the structural, dynamical and rheological properties of colloid-polymer mixtures with an intermediate colloid volume fraction, $\phi=0.4$, as a function of increasing polymer concentration, corresponding to increasing interparticle attraction. These samples covered a broad range from liquids to gels.

The structure of the samples was investigated by SLS and microscopy. Within the liquid we observed the formation of increasingly larger structures, especially when approaching the gelation boundary. Increasing attraction induces the formation of particle clusters which, at sufficiently large attraction, interconnect to form a space-spanning network. The maximum cluster size and maximum structural heterogeneity is observed at the gelation boundary. Within the gel region, increasing attraction leads to a more uniform structure with a reduction in the characteristic length scale. This trend is reminiscent of critical behavior expected for phase separation that is arrested by gelation and is in agreement with studies on similar colloid-polymer mixtures.^{42–44,77}

Within the entire liquid phase, the dynamics show an ergodic response. Upon approaching gelation, the short-time (in-bond) diffusion as well as the long-time diffusion, which leads to the final structural relaxation of the system, slows down. The more pronounced slowing down of the long-time decay indicates the approach of gelation and its increasingly stretched exponential form suggests that heterogeneities in the density fluctuations are increased and the distribution of length scales is broadened, reminiscent of clustering. This is consistent with the increasing correlation length observed in SLS and microscopy. This suggests that structural and dynamical heterogeneities, namely, clustering and the formation of transient networks, are precursors of gel formation. The coincidence of structural and dynamical heterogeneity observed here agrees with the behavior observed at lower volume fraction for the same system.^{43,45}

Rheological measurements in the linear viscoelastic regime show, with increasing polymer concentration, a shifting of the crossing point of the elastic and viscous moduli corresponding to a transition from a liquidlike to a gel-like response at a characteristic frequency (time). This characteristic time could for the first time be related to the “bond” lifetime estimated by the time needed to escape from the interparticle attraction. Bond breaking was found to be the

dominating process close to the gelation boundary, while at lower polymer concentrations the relaxation appears to be related to particle or cluster diffusion.

The elastic modulus of samples approaching the gelation boundary has been compared to MCT predictions within the $F_{12}^{(\dot{\gamma})}$ model.⁵⁶ The predictions reproduce the dependence of the modulus at fixed frequency on attraction strength, i.e., polymer concentration. However, the full frequency dependence of the modulus shows discrepancies. This could be due to dynamical heterogeneities, which are not included in the theory.

We compared the dependence of the elastic modulus on polymer concentration also to MCT-PRISM predictions, previously used to describe the same dependence in silica-PS mixtures.³⁸ Comparison between experiment and theory requires a consistent definition of the gelation boundary and/or a scaling factor. With an appropriate choice, fair agreement can be obtained in a limited range of polymer concentrations, i.e., attraction strengths, a range which is comparable to the one investigated for silica-PS mixtures. In silica-PS gels, the need for a scaling factor was related to the size of heterogeneities, which are not considered by theory.³⁸ In contrast, in our system the need for rescaling is closely related to the choice of the gelation boundary. The different behavior of our system compared to silica-PS mixtures is attributed to specific properties of the two systems, such as the different degrees of “softness” of the particles, different interactions between polymer and particle surface, and a different importance of gravity.

In the gel region, the shear moduli show a solidlike behavior, with G' weakly frequency dependent and always larger than G'' , which shows a minimum in the frequency dependence. At fixed frequency, G' increases almost linearly with polymer concentration. We suggest that this is consistent with a fractal model for gel elasticity in the so-called weak-link regime (similar to low volume fraction gels^{10,19,92}). Within this model, the almost linear dependence of G' results from the increase of the energy of intercluster links with increasing polymer concentration, while at the same time, the cluster size in the gel remains approximately constant. This implies that due to the heterogeneous structure of the samples, the elasticity of the gels is dominated by cluster-cluster links rather than particle-particle bonds.

ACKNOWLEDGMENTS

This work was funded by the Deutsche Forschungsgemeinschaft (DFG) within the German-Dutch Collaborative Research Centre Sonderforschungsbereich-Transregio 6 (SFB-TR6), Project Section A6. The Düsseldorf-Crete collaboration was supported by the EU Network of Excellence “SoftComp.” M. Laurati would like to acknowledge E. Zaccarelli for stimulating discussions. G. Petekidis and N. Koumakis acknowledge funding by the EU Transfer of Knowledge “Cosines” and the Greek General Secretariat for Research through PENED Grant No. 03EΔ566.

¹R. G. Larson, *The Structure and Rheology of Complex Fluids* (Oxford University Press, New York, 1999).

²P. Coussot, *Rheometry of Pastes, Suspensions and Granular Materials*

(Wiley, New York, 2005).

- ³P. N. Pusey, *Liquids, Freezing and Glass Transition* (North-Holland, Amsterdam, 1991).
- ⁴W. C. K. Poon, *Science* **30**, 4830 (2004).
- ⁵W. C. K. Poon, *J. Phys.: Condens. Matter* **14**, R859 (2002).
- ⁶S. A. Shah, Y. L. Chen, K. S. Schweizer, and C. F. Zukoski, *J. Chem. Phys.* **118**, 3350 (2003).
- ⁷A. Stradner, H. Sedgwick, F. Cardinaux, W. C. K. Poon, S. U. Egelhaaf, and P. Schurtenberger, *Nature (London)* **432**, 492 (2004).
- ⁸H. Sedgwick, S. U. Egelhaaf, and W. C. K. Poon, *J. Phys.: Condens. Matter* **16**, S4913 (2004).
- ⁹H. Sedgwick, K. Kroy, A. Salonen, M. B. Robertson, S. U. Egelhaaf, and W. C. K. Poon, *Eur. Phys. J. E* **16**, 77 (2005).
- ¹⁰A. H. Krall and D. A. Weitz, *Phys. Rev. Lett.* **80**, 778 (1998).
- ¹¹P. J. Lu, J. C. Conrad, H. M. Wyss, A. B. Schofield, and D. A. Weitz, *Phys. Rev. Lett.* **96**, 028306 (2006).
- ¹²P. J. Lu, E. Zaccarelli, F. Ciulla, A. B. Schofield, F. Sciortino, and D. A. Weitz, *Nature (London)* **453**, 499 (2008).
- ¹³H. Verduin and J. K. G. Dhont, *J. Colloid Interface Sci.* **172**, 425 (1995).
- ¹⁴S. M. Ilett, A. Orrock, W. C. K. Poon, and P. N. Pusey, *Phys. Rev. E* **51**, 1344 (1995).
- ¹⁵W. C. K. Poon, A. D. Pirie, M. D. Haw, and P. N. Pusey, *Physica A* **235**, 110 (1997).
- ¹⁶N. A. M. Verhaegh, D. Asnaghi, H. N. W. Lekkerkerker, M. Giglio, and L. Cipelletti, *Physica A* **242**, 104 (1997).
- ¹⁷S. Manley, H. Wyss, K. Miyazaki, J. Conrad, V. Trappe, L. J. Kaufmann, D. R. Reichmann, and D. A. Weitz, *Phys. Rev. Lett.* **95**, 238302 (2005).
- ¹⁸F. Cardinaux, T. Gibaud, A. Stradner, and P. Schurtenberger, *Phys. Rev. Lett.* **99**, 118301 (2007).
- ¹⁹V. Trappe and D. A. Weitz, *Phys. Rev. Lett.* **85**, 449 (2000).
- ²⁰M. H. Lee and E. M. Furst, *Phys. Rev. E* **77**, 041408 (2008).
- ²¹E. M. Furst and J. P. Pantina, *Phys. Rev. E* **75**, 050402 (2007).
- ²²P. N. Pusey and W. van Meegen, *Nature (London)* **320**, 340 (1986).
- ²³P. N. Pusey and W. van Meegen, *Phys. Rev. Lett.* **59**, 2083 (1987).
- ²⁴K. N. Pham, A. M. Puertas, J. Bergenholtz, S. U. Egelhaaf, A. Moussaid, P. N. Pusey, A. B. Schofield, M. Cates, M. Fuchs, and W. C. K. Poon, *Science* **296**, 104 (2002).
- ²⁵T. Eckert and E. Bartsch, *Phys. Rev. Lett.* **89**, 125701 (2002).
- ²⁶K. A. Dawson, G. Foffi, M. Fuchs, W. Götze, F. Sciortino, M. Sperl, P. Tartaglia, T. Voigtman, and E. Zaccarelli, *Phys. Rev. E* **63**, 011401 (2001).
- ²⁷W. van Meegen and S. M. Underwood, *Phys. Rev. E* **47**, 248 (1993).
- ²⁸W. van Meegen and S. M. Underwood, *Phys. Rev. E* **49**, 4206 (1994).
- ²⁹M. E. Cates, *Ann. Henri Poincaré* **2**, S647 (2003).
- ³⁰T. G. Mason and D. A. Weitz, *Phys. Rev. Lett.* **75**, 2770 (1995).
- ³¹J. Bergenholtz, W. C. K. Poon, and M. Fuchs, *Langmuir* **19**, 4493 (2003).
- ³²G. Petekidis, A. Moussaid, and P. N. Pusey, *Phys. Rev. E* **66**, 051402 (2002).
- ³³G. Petekidis, D. Vlassopoulos, and P. N. Pusey, *J. Phys.: Condens. Matter* **16**, S3955 (2004).
- ³⁴K. N. Pham, G. Petekidis, D. Vlassopoulos, S. U. Egelhaaf, P. N. Pusey, and W. C. K. Poon, *Europhys. Lett.* **75**, 624 (2006).
- ³⁵K. N. Pham, G. Petekidis, D. Vlassopoulos, S. U. Egelhaaf, W. C. K. Poon, and P. N. Pusey, *J. Rheol.* **52**, 649 (2008).
- ³⁶E. Zaccarelli, *J. Phys.: Condens. Matter* **19**, 323101 (2007).
- ³⁷J. Vermant and M. J. Solomon, *J. Phys.: Condens. Matter* **17**, R187 (2005).
- ³⁸S. A. Shah, Y. L. Chen, K. S. Schweizer, and C. F. Zukoski, *J. Chem. Phys.* **119**, 8747 (2003).
- ³⁹J. Bergenholtz and M. Fuchs, *Phys. Rev. E* **59**, 5706 (1999).
- ⁴⁰S. A. Shah, Y. L. Chen, S. Ramakrishnan, K. S. Schweizer, and C. F. Zukoski, *J. Phys.: Condens. Matter* **15**, 4751 (2003).
- ⁴¹K. F. Seefeldt and M. J. Solomon, *Phys. Rev. E* **67**, 050402 (2003).
- ⁴²P. Varadan and M. J. Solomon, *Langmuir* **19**, 509 (2003).
- ⁴³C. J. Dibble, M. Kogan, and M. J. Solomon, *Phys. Rev. E* **74**, 041403 (2006).
- ⁴⁴P. A. Smith, G. Petekidis, S. U. Egelhaaf, and W. C. K. Poon, *Phys. Rev. E* **76**, 041402 (2007).
- ⁴⁵C. J. Dibble, M. Kogan, and M. J. Solomon, *Phys. Rev. E* **77**, 050401 (2008).
- ⁴⁶M. Fuchs and K. S. Schweizer, *J. Phys.: Condens. Matter* **14**, R239 (2002).
- ⁴⁷A. M. Puertas, M. Fuchs, and M. E. Cates, *J. Chem. Phys.* **121**, 2813 (2004).

- ⁴⁸M. H. Lee and E. M. Furst, *Phys. Rev. E* **77**, 041408 (2008).
- ⁴⁹V. J. Anderson and H. N. W. Lekkerkerker, *Nature (London)* **416**, 811 (2002).
- ⁵⁰A. P. Gast, C. K. Hall, and W. B. Russell, *J. Colloid Interface Sci.* **96**, 251 (1983).
- ⁵¹B. Vincent, J. Edwards, S. Emmett, and R. Croot, *Colloids Surf.* **31**, 267 (1988).
- ⁵²W. C. K. Poon, L. Starrs, S. P. Meeker, A. Moussaid, R. M. L. Evans, P. N. Pusey, and M. M. Robins, *Faraday Discuss.* **112**, 143 (1999).
- ⁵³L. Starrs, W. C. K. Poon, D. J. Hibberd, and M. M. Robins, *J. Phys.: Condens. Matter* **14**, 2485 (2002).
- ⁵⁴M. Fuchs and M. Ballauff, *J. Chem. Phys.* **122**, 094707 (2005).
- ⁵⁵M. Fuchs and M. E. Cates, *Phys. Rev. Lett.* **89**, 248304 (2002).
- ⁵⁶M. Fuchs and M. E. Cates, *Faraday Discuss.* **123**, 267 (2003).
- ⁵⁷J. M. Brader, T. Voigtmann, M. E. Cates, and M. Fuchs, *Phys. Rev. Lett.* **98**, 058301 (2007).
- ⁵⁸A. V. Indrani and S. Ramaswamy, *Phys. Rev. E* **52**, 6492 (1995).
- ⁵⁹K. Miyazaki and D. R. Reichman, *Phys. Rev. E* **66**, 050501 (2002).
- ⁶⁰K. Miyazaki, H. M. Wyss, D. A. Weitz, and D. R. Reichman, *Europhys. Lett.* **75**, 915 (2006).
- ⁶¹J. Zausch, J. Horbach, M. Laurati, S. U. Egelhaaf, J. M. Brader, T. Voigtmann, and M. Fuchs, *J. Phys.: Condens. Matter* **20**, 404210 (2008).
- ⁶²J. M. Brader, M. E. Cates, and M. Fuchs, *Phys. Rev. Lett.* **101**, 138301 (2008).
- ⁶³G. C. Berry, *J. Chem. Phys.* **44**, 4550 (1966).
- ⁶⁴G. J. Fleer and R. Tuinier, *Phys. Rev. E* **76**, 041802 (2007).
- ⁶⁵H. N. W. Lekkerkerker, W. C. K. Poon, P. N. Pusey, A. Stroobants, and P. B. Warren, *Europhys. Lett.* **20**, 559 (1992).
- ⁶⁶W. Schaertl and H. Silesco, *J. Stat. Phys.* **77**, 1007 (1994).
- ⁶⁷D. G. A. L. Aarts, R. Tuinier, and H. N. W. Lekkerkerker, *J. Phys.: Condens. Matter* **14**, 7551 (2002).
- ⁶⁸K. Schätzel, *J. Mod. Opt.* **38**, 1849 (1991).
- ⁶⁹C. Urban and P. Schurtenberger, *J. Colloid Interface Sci.* **207**, 150 (1998).
- ⁷⁰K. N. Pham, S. U. Egelhaaf, P. N. Pusey, and W. C. K. Poon, *Phys. Rev. E* **69**, 011503 (2004).
- ⁷¹K. D. Horner, M. Topper, and M. Ballauff, *Langmuir* **13**, 551 (1997).
- ⁷²M. C. Jenkins and S. U. Egelhaaf, *Adv. Colloid Interface Sci.* **136**, 65 (2008).
- ⁷³M. Laurati, G. Petekidis, and S. U. Egelhaaf (unpublished).
- ⁷⁴N. Koumakis and G. Petekidis (unpublished).
- ⁷⁵C. G. De Kruijff, W. J. Briels, R. P. May, and A. Vrij, *Langmuir* **4**, 668 (1988).
- ⁷⁶J. S. Higgins and H. C. Benoit, *Polymers and Neutron Scattering* (Oxford University Press, Oxford, 1994).
- ⁷⁷P. A. Smith, Ph.D. thesis, University of Edinburgh, 2004.
- ⁷⁸P. Voudouris, B. Loppinet, and G. Petekidis, *Phys. Rev. E* **77**, 051402 (2008).
- ⁷⁹T. Shikata and D. S. Pearson, *J. Rheol.* **38**, 601 (1994).
- ⁸⁰F. Chambon, Z. S. Petrovic, W. J. MacKnight, and H. H. Winter, *Macromolecules* **19**, 2146 (1986).
- ⁸¹H. H. Winter and F. Chambon, *J. Rheol.* **30**, 367 (1986).
- ⁸²H. W. Richtering, K. D. Gagnon, R. W. Lenz, R. C. Fuller, and H. H. Winter, *Macromolecules* **25**, 2429 (1992).
- ⁸³P. Sollich, *Phys. Rev. E* **58**, 738 (1998).
- ⁸⁴T. G. Mason, J. Bibette, and D. A. Weitz, *Phys. Rev. Lett.* **75**, 2051 (1995).
- ⁸⁵M. Cloitre, R. Borrega, and L. Leibler, *Phys. Rev. Lett.* **85**, 4819 (2000).
- ⁸⁶R. J. Ketz, R. K. Prudhomme, and W. W. Graessley, *Rheol. Acta* **27**, 531 (1988).
- ⁸⁷M. R. Mackley, R. T. J. Marshall, J. B. A. F. Smeulders, and F. D. Zhao, *Chem. Eng. Sci.* **49**, 2551 (1994).
- ⁸⁸N. Koumakis, A. B. Schofield, and G. Petekidis, *Soft Matter* **4**, 2008 (2008).
- ⁸⁹H. A. Kramers, *Physica A* **7**, 284 (1940).
- ⁹⁰T. McLeish, *Soft and Fragile Matter, Non Equilibrium Dynamics, Metastability and Flow* (Institute of Physics, Bristol, 2000).
- ⁹¹W. Götze, *Liquids, Freezing and Glass Transition* (North-Holland, Amsterdam, 1991).
- ⁹²W.-H. Shih, W. Y. Shih, S.-I. Kim, J. Liu, and I. A. Aksay, *Phys. Rev. A* **42**, 4772 (1990).
- ⁹³S. S. Narine and A. G. Marangoni, *Phys. Rev. E* **60**, 6991 (1999).
- ⁹⁴H. Wu and M. Morbidelli, *Langmuir* **17**, 1030 (2001).